

Annual and seasonal mean buoyancy fluxes for the tropical Indian Ocean

T. G. Prasad

Physical Oceanography Division, National Institute of Oceanography, Dona Paula, Goa 403 004, India
Present address: C-CADD, National Aerospace Laboratories, Belur Campus, Bangalore 560 037, India

INSAT-derived monthly mean precipitation, combined with estimates of evaporation from COADS, are used to prepare the annual mean and seasonal distributions of evaporation-precipitation ($E-P$) and buoyancy fluxes for the tropical Indian Ocean. The fluxes of heat and freshwater across the air-sea interface, and hence the surface buoyancy flux, show strong spatial and temporal variability. The Bay of Bengal and eastern equatorial Indian Ocean are characterized by a net freshwater gain due to heavy precipitation, while the northern Arabian Sea and the ocean south of 10°S experience a net loss of freshwater due to excessive evaporation. The regions of high and low salt flux broadly correspond to those of high and low $E-P$ and the seasonal fluctuations of $E-P$ appear to contribute to the seasonal cycle of salt flux. The buoyancy flux is dominated by strong density loss by the ocean in the northern Indian Ocean and modest density gain in the southern Indian Ocean. Though heat flux is the dominant contributor to the buoyancy flux over most of the region, salt flux dominates during winter in the northern Arabian Sea and during summer and fall in the Bay of Bengal and the eastern equatorial Indian Ocean.

THE tropical Indian Ocean, with its unique seasonal reversing monsoons, land locked in the north and open to the south, represents an area of intense air-sea interaction. The Arabian Sea and the Bay of Bengal show marked difference in their climatic conditions even though they occupy the same latitude belt. The annual winds are the basic physical forcing that brings in large spatio-temporal variations of the surface waters which in turn regulate various processes in the Arabian Sea and the Bay of Bengal including the upper ocean circulation and the temperature and salinity fields. The changes in the heat and freshwater fluxes across the air-sea surface bring about changes in the surface buoyancy flux. Differential surface buoyancy fluxes induce horizontal pressure gradients, which in turn alter the topography of the isobaric surfaces and thereby the circulation patterns¹⁻³. The impact of these pressure forces on the ocean dynamics depends on the magnitude and scale of the heat and freshwater fluxes, which depends on the scales of the atmospheric process responsible for the

fluxes. Apart from these, there is a throughflow of warm freshwater from the western Pacific Warm Pool into the equatorial Indian Ocean.

Information on freshwater flux for the tropical Indian Ocean is scanty. The maps presented by Baumgartner and Reichel⁴ give only long term annual averages of E , P and $E-P$ in the tropical Indian Ocean, which are based on extrapolation of island and coastal station measurements, with reasonable adjustments for uplands. So, it is worthwhile to undertake an estimate of $E-P$ and buoyancy fluxes for the tropical Indian Ocean, to determine the dominant processes contributing to the surface buoyancy flux.

We discuss here the relative contributions of heat and salt flux to the total surface buoyancy flux in the tropical Indian Ocean. The annual and seasonal distributions of $E-P$ and buoyancy flux for the tropical Indian Ocean are presented and discussed. The contributions of both the thermal and haline components of the flux are presented separately, and also as a ratio. The implications of the buoyancy flux for water mass formation are discussed.

Data source and analysis

To derive monthly mean values of surface heat flux and evaporation, the observations from the Comprehensive Ocean Atmosphere Data Set (COADS)⁵ have been used. The surface fluxes (Wm^{-2}) were calculated by using standard bulk aerodynamic formulae⁶, for latent (Q_e) and sensible (conductive) (Q_s) heat exchange:

$$Q_e = \rho L C_e (q_s - q_a) U,$$

$$Q_s = \rho C_p C_s (T_w - T_a) U,$$

where L is the latent heat of vaporization, C_p the specific heat of water, q the specific humidity, C_e and C_s empirical exchange coefficients (1.4×10^{-3}), T_w the sea surface temperature, T_a the air temperature and U the wind speed. The evaporation is computed by using the equation $E = \rho C_e (q_s - q_a) U$.

The Very High Resolution Radiometer (VHRR) onboard the Indian National SATellite (INSAT) was used for deriving the precipitation estimates. The present es-

RESEARCH ARTICLES

imates of monthly rainfall for the tropical Indian Ocean were extracted for the region north of 20°S and west of 100°E on a 2.5° × 2.5° grid. The methodology used for deriving the quantitative precipitation estimates is after Rao *et al.*⁷ and Ramesh Kumar and Prasad⁸.

The surface buoyancy flux has two components, one due to the net heat flux and the other due to the freshwater flux associated with evaporation and precipitation. The buoyancy flux F_ρ is given by,

$$F_\rho = -\rho(\alpha F_T - \beta F_S),$$

where ρ is the density, and F_T and F_S the fluxes due to heat and salt; the thermal expansion (α) and the haline contraction (β) coefficients are defined as:

$$\alpha = -\frac{1}{\rho} \left. \frac{\partial \rho}{\partial T} \right|_{P,S}, \quad \beta = \frac{1}{\rho} \left. \frac{\partial \rho}{\partial S} \right|_{P,T}.$$

The heat flux is given by $F_T = Q(\rho C_p)^{-1}$, where Q is the net heat flux into the ocean and ρC_p is the heat capacity of water⁹. The salt flux is due to the loss of freshwater from the sea surface and is obtained by noting that a freshwater flow from the sea surface at a rate of $E-P$

must be supplied by a slightly larger flow of salt water (with salinity: S) below the sea surface equal to $(E-P)/(1-S)$ (ref. 10). Salt is left behind by this flow at a rate equal to $(E-P)S/(1-S)$ and is carried by turbulence and diffusion back into the ocean interior. The surface salt flux is then:

$$F_S = (E - P)S/(1 - S).$$

The expansion coefficients, heat capacity and density were evaluated using surface temperature and salinity extracted from the National Oceanographic Data Center¹¹ (NODC), CD-ROM north of 20°S, and west of 100°E.

The INSAT-derived precipitation, combined with evaporation, was used to prepare the annual and seasonal distributions of evaporation-precipitation ($E-P$). The monthly mean data were then averaged into seasonal and annual estimates. The seasonal maps are presented for winter (December-February), spring (March-May), summer (June-August) and fall (September-November).

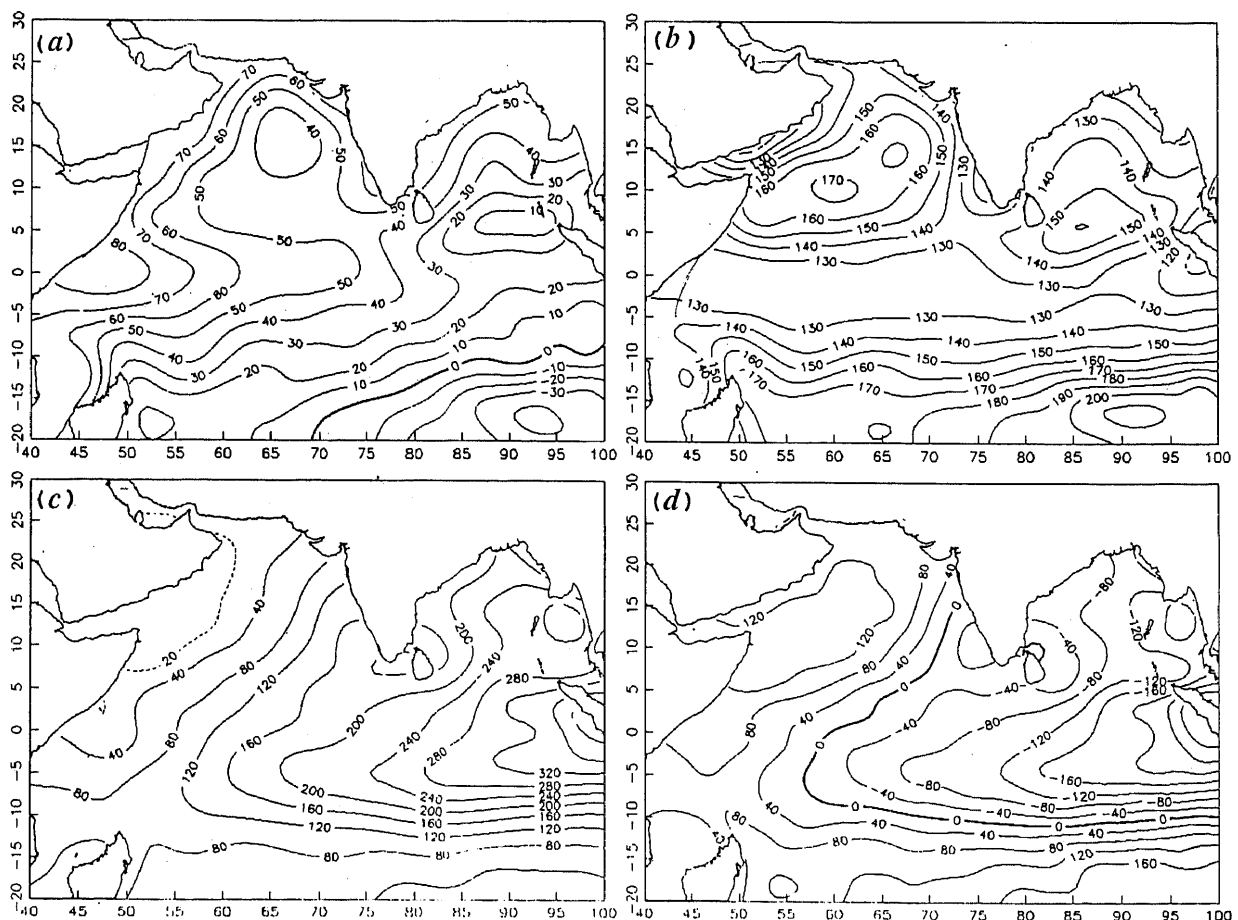


Figure 1. Annual mean distributions of (a) Net oceanic heat flux (W m^{-2}); (b) Evaporation (cm yr^{-1}); (c) Precipitation (cm yr^{-1}); and (d) Evaporation-Precipitation ($E-P$, cm yr^{-1}).

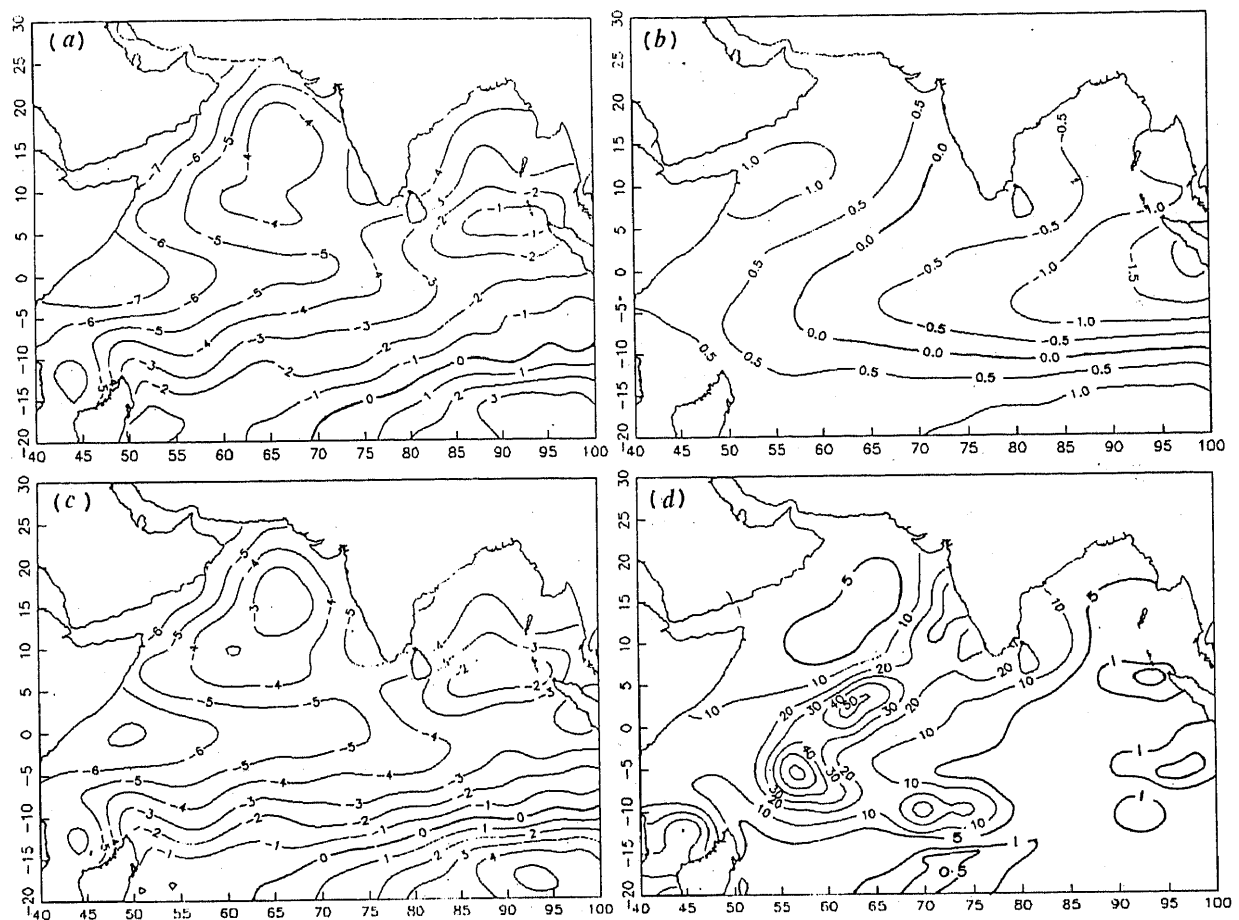


Figure 2. Annual mean distributions of (a) Thermal buoyancy flux into the ocean ($-\rho\Delta F_T$) in $10^{-6} \text{ kg (m}^2\text{s)}^{-1}$; (b) Haline buoyancy flux into the ocean ($\rho\beta F_S$) in $10^{-6} \text{ kg (m}^2\text{s)}^{-1}$; (c) the total buoyancy flux in $10^{-6} \text{ kg (m}^2\text{s)}^{-1}$; (d) $|\Delta F_T/\beta F_S|$.

Results and discussion

Annual mean distributions

Heat flux. Figure 1a depicts the annual mean net heat flux. The central Arabian Sea and region west of Sumatra is characterized by a minimum heat gain, while region south of 10°S , at the south-east extremity shows net heat release from the ocean to the atmosphere. Heat uptake of the ocean is dominant in the upwelling regions off the coasts of Africa and Arabia. The average annual heat input in the equatorial region shows an east-west gradient with a high off eastern Africa. It appears that the tropical Indian Ocean gains heat from the atmosphere on an annual average and a cold water inflow below the surface is expected by advective transport to conserve heat balance in the basin.

Evaporation. Figure 1b shows the annual mean evaporation. A zone of minimum evaporation is observed in the equatorial band between 5°S and 5°N . Evaporation is minimum along the west coast of India, off the Arabian coasts and over the Bay of Bengal. The Arabian

Sea, particularly central Arabian Sea, is characterized by high evaporation rate. South of 5°S , the evaporation increases towards south.

Precipitation. The annual precipitation over the tropical Indian Ocean is illustrated in Figure 1c. Precipitation over the equatorial region shows a maximum off Indonesia, with a tongue extending westward. The Bay of Bengal receives three times as much precipitation as the Arabian Sea. The decreases in precipitation toward south in the southern Indian Ocean is zonal on account of the zonal cloud pattern and the corresponding predominant zonal temperature distribution.

There is close agreement (in amounts and features) between the present annual rainfall estimates and the climatological map of Baumgartner and Reichel⁴. Further, the present estimates compare reasonably well with the climatological study of Jaeger¹² and the satellite microwave estimates of Martin *et al.*¹³ and Rao *et al.*¹⁴.

Evaporation-precipitation (E-P). The freshwater flux across the air-sea interface is defined as the difference

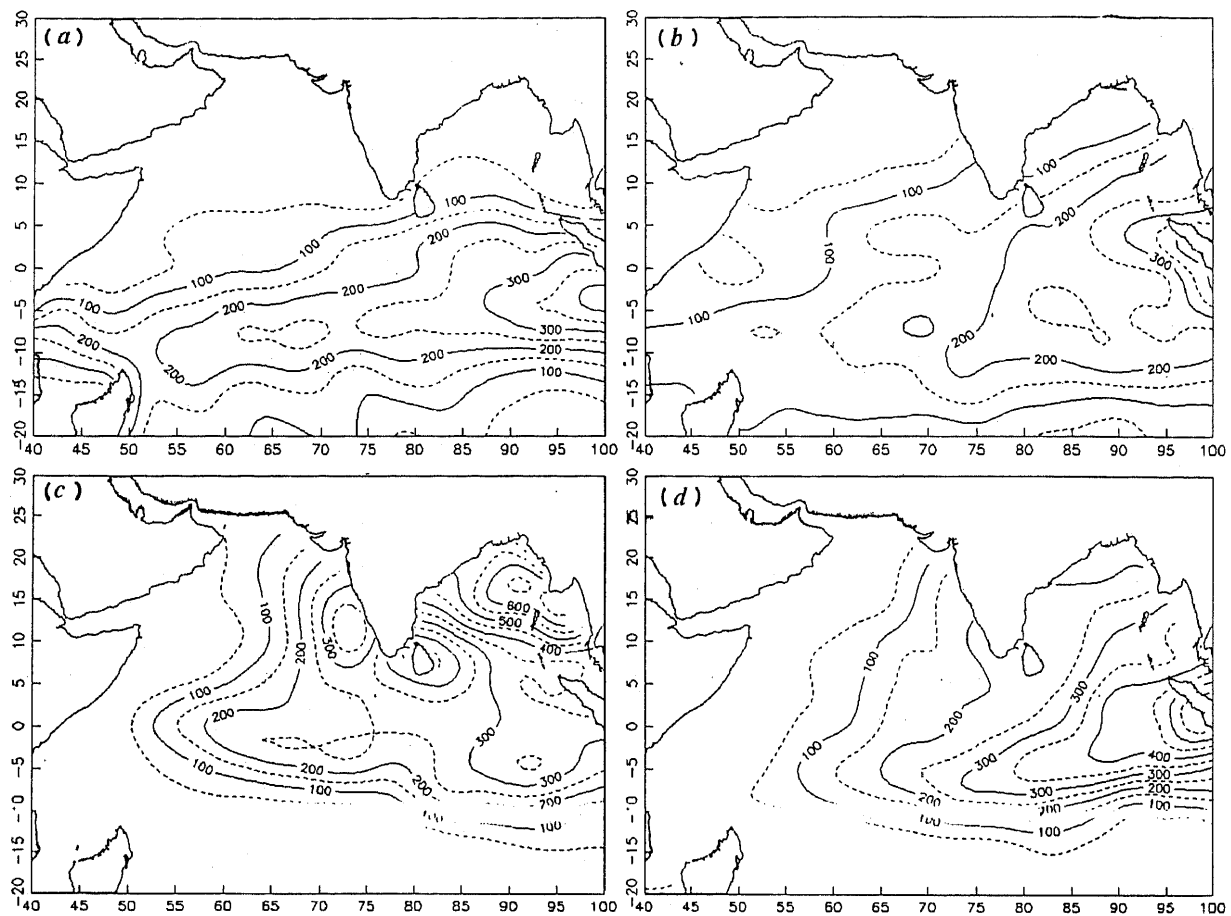


Figure 3. Seasonal precipitation (cm yr^{-1}) based on INSAT data for (a) Winter (December–February); (b) Spring (March–May); (c) Summer (June–August); and (d) Fall (September–November).

of evaporation and precipitation ($E-P$). The annual distribution of $E-P$ is illustrated in Figure 1d. The features in the annual map of $E-P$ are in good agreement with the climatological estimates of $E-P$ provided by Baumgartner and Reichel⁴. Precipitation exceeds evaporative losses in the equatorial region, particularly off Indonesia, and over the Bay of Bengal. The maximum freshwater gain (-280 cm yr^{-1}) in the equatorial region is three times larger than the corresponding extrema over the Bay of Bengal (-80 cm yr^{-1}). The decrease in freshwater flux toward west in the equatorial region can be associated with east–west gradient of precipitation. Evaporation is dominant in the north-western Arabian Sea, particularly off Arabia, and south of 15°S . The strong north–south gradient of $E-P$ seen in the southern Indian Ocean between 5°S and 15°S is due to the moisture convergence at 10°S . In general, the annual precipitation is high in the equatorial belt, Bay of Bengal and along the west coast of India, whereas the north-western Arabian Sea and region south of 15°S experience a net evaporative heat loss.

Buoyancy flux. Figure 2a, b depicts the separate contribution of heat ($-\rho\alpha F_T$) and salt flux ($\rho\beta F_S$) to the total buoyancy flux (Figure 2c) respectively. It is interesting to note that the thermal buoyancy flux shows dominance over most of the area. The buoyancy flux due to salt has strong resemblance to the $E-P$ distribution. Areas of salt gain are seen in the northern Arabian Sea and south of 10°S , which is expected to be the region of high evaporative heat loss as could be seen from fluxes of heat and freshwater distribution. The excess precipitation over evaporation in the Bay of Bengal and equatorial region, particularly far east, causes freshening of surface salinity leading to salt loss. Thus, it can be concluded that the regions of high and low salt flux broadly correspond to those of high and low $E-P$. The distribution of annual surface buoyancy flux (Figure 2c) has strong similarities to the net heat flux. The regions of strongest density gain are in the south-east, where the cold air masses blow over relatively warm waters of South Equatorial Current. This region corresponds to expected areas of heat loss due to evaporative cooling under the influence

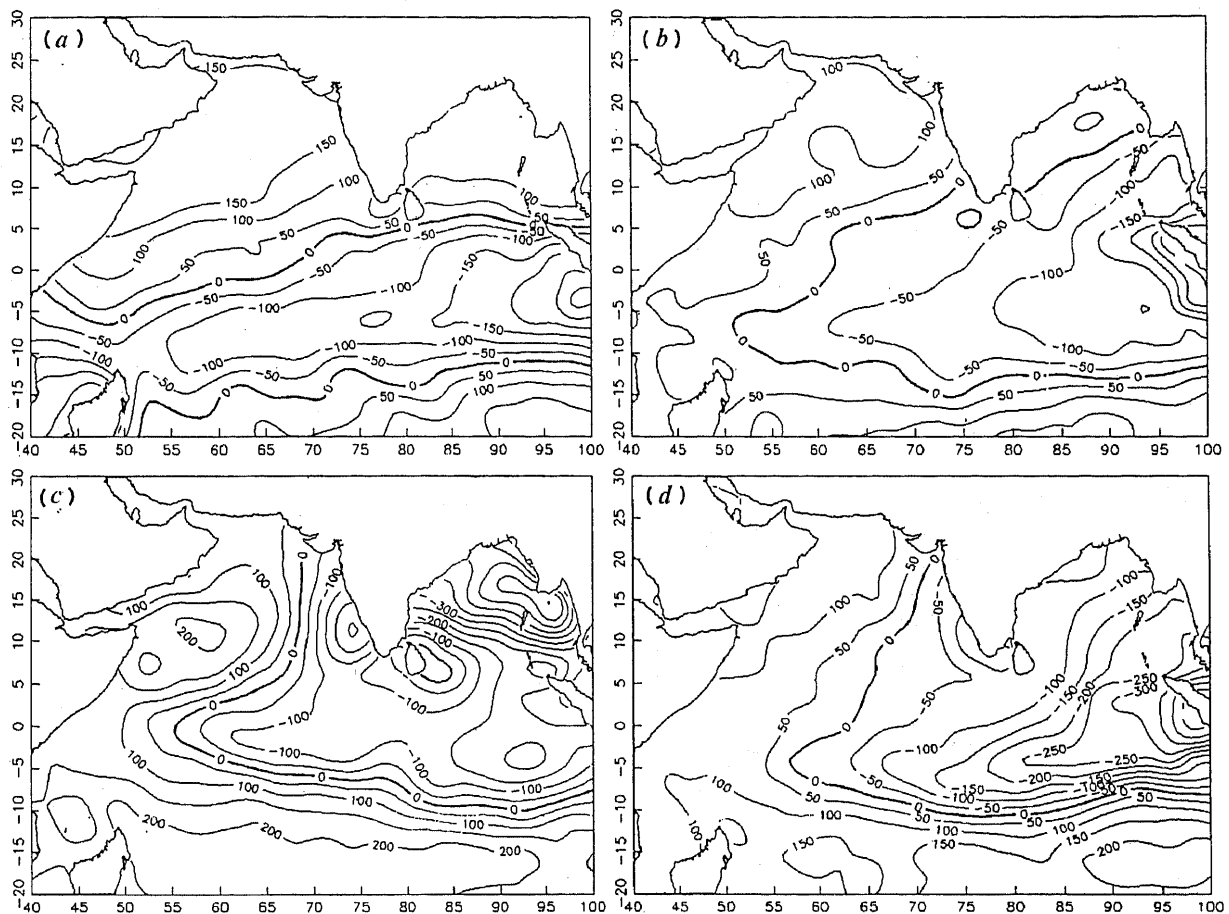


Figure 4. Seasonal distribution of $E-P$ (cm yr^{-1}) for (a) Winter (December–February); (b) Spring (March–May); (c) Summer (June–August); and (d) Fall (September–November)

of south east trade winds. High values of density loss are found in the equatorial and along the upwelling regions. The dominance of these components can be delineated from the absolute value of ratio of the heat to salt flux $|\alpha F_T / \beta F_S|$ (Figure 2 d). The most interesting feature of the flux ratio distribution is that the heat flux dominates in the whole tropical Indian Ocean.

Seasonal mean distributions

Precipitation. Figures 3 a–d depict seasonal distribution of precipitation for winter (DJF), spring (MAM), summer (JJA), and fall (SON) respectively. A maximum in precipitation occurs off Indonesia in winter, spring, and fall with a tongue westward. During summer, the period of the southwest monsoon, the maximum shifts north and intensifies in the Bay of Bengal, with a secondary maximum off the west coast of India. Interestingly, the precipitation pattern in the Arabian Sea during summer and fall months is oriented north-east on account of prevailing winds in these regions.

Evaporation–precipitation ($E-P$). The seasonal estimates of $E-P$ rate are presented in Figures 4 a–d. During

winter, there is a net loss of freshwater from the Arabian Sea, Bay of Bengal and the region south of 15°S due to excess evaporation, and a net freshwater gain in the equatorial region, with a maximum off Indonesia. Interestingly, the freshwater loss from the Arabian Sea is nearly twice that from the Bay of Bengal.

Spring and fall show a decrease in freshwater flux on an average with a maximum freshwater gain in the eastern equatorial Indian Ocean during fall. The decrease of $E-P$ in the equatorial region can be associated with east–west gradient of precipitation.

As expected, the onset of southwest monsoon winds bring about a marked increase in precipitation over the Bay of Bengal, equatorial Indian Ocean and along the west coast of India. The north-western Arabian Sea and the region south of 10°S receive the least precipitation; this along with enhanced evaporation leads to a net loss of freshwater from the surface.

Buoyancy flux. Figures 5 a–d illustrate the total surface buoyancy flux for winter, spring, summer and fall months respectively. During winter, north-western Arabian Sea experiences density gain due to evaporative cooling with concomitant heat loss and essentially no

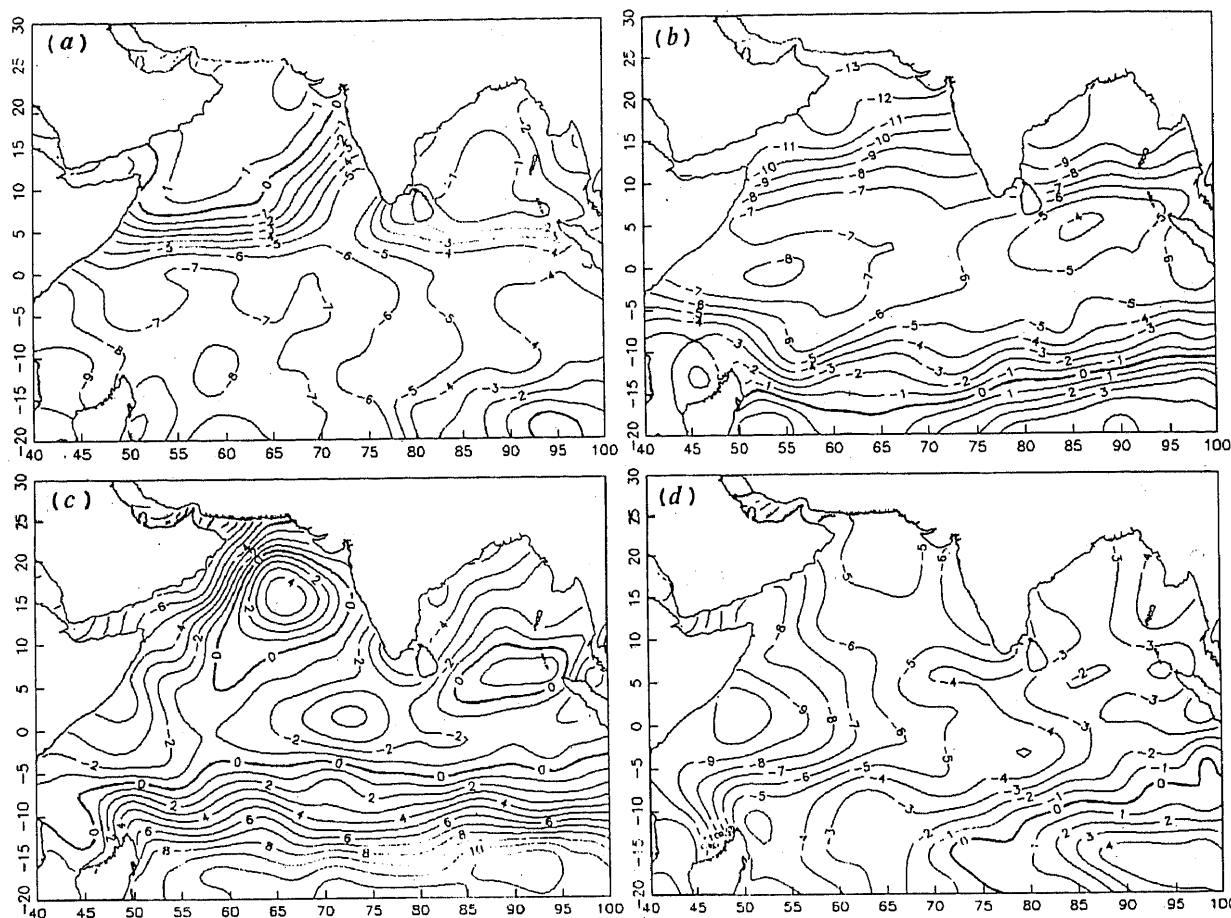


Figure 5. Seasonal distribution of surface buoyancy flux in $10^{-6} \text{ kg (m}^2\text{s)}^{-1}$ for (a) Winter (December–February); (b) Spring (March–May); (c) Summer (June–August); and (d) Fall (September–November).

precipitation. Density gain due to excess evaporation in the northern Arabian Sea leads to the formation of Arabian Sea High Salinity Water mass (36.5 PSU), which sinks and spreads towards south with the advance of the northeast monsoon³. The sharp gradient of buoyancy flux seen in the Arabian Sea is due to the advection of low salinity water from the Bay of Bengal, carried by the North Equatorial Current, and the southward extension of Arabian Sea High Salinity Water mass. The increase in buoyancy flux toward west in the equatorial region can be associated with east-west gradient of distribution of heat and freshwater fluxes. Areas of strong density loss in the equatorial region coincide with areas of net heat and freshwater fluxes into the ocean.

During spring, the whole tropical Indian Ocean north of 15°S experiences density loss, with strongest losses seen in the northern Arabian Sea and Bay of Bengal. This corresponds to a region of heat gain due to intense solar heating, along with weak winds and comparatively less precipitation. It is to be noted that the region south of 15°S shows a net density gain due to evaporative cooling under the influence of south-east trade winds.

A maximum in density gain occurs in the southern Indian Ocean, south of 5°S during summer, on account of evaporative heat loss under the influence of south-east trade winds. The two regions of density gain are in the northern Indian Ocean, a maximum in the central Arabian Sea, a region of heat loss caused by high evaporation under strong low-level Findlater jet, with a secondary maximum in the north-west of Sumatra. Regions of density loss are seen off Somalia, Arabia and northern extremity of Arabian Sea. These are regions of oceanic upwelling where denser water is brought to the surface.

During fall, most of the region shows buoyancy loss due to solar heating except in the southern extremity. It is worth noting that the heat flux during this season shows a meridional gradient with maximum heat flux coinciding with the area of maximum buoyancy loss.

Figures 6a–d depict seasonal distribution of the absolute value of the ratio of the heat to salt flux $|\alpha F_T/\beta F_S|$. The most interesting feature of the flux ratio distribution during winter is the dominance of salt flux in the north-western Arabian Sea, the eastern equatorial Indian

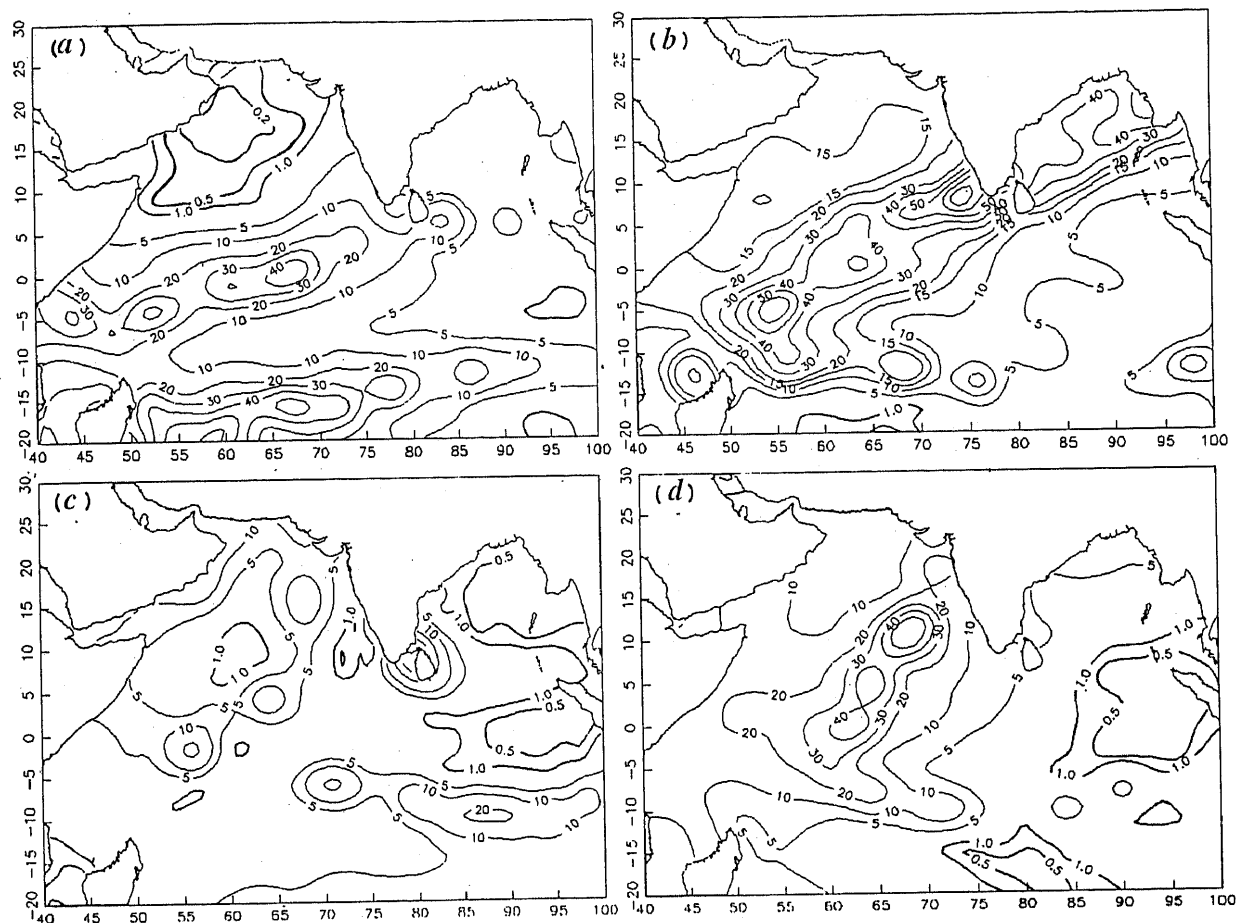


Figure 6. Seasonal distribution of $|\alpha F_T / \beta F_S|$ for (a) Winter (December–February); (b) Spring (March–May); (c) Summer (June–August); and (d) Fall (September–November).

Ocean and the Bay of Bengal. The buoyancy flux due to heat exceeds that due to salt in the tropical Indian Ocean during spring. This is the manifestation of heat flux into the ocean due to intense solar heating at the sea surface. Interestingly, during summer, the buoyancy flux due to heat and salt fluxes are almost equal; the salt flux dominates in the Bay of Bengal, off the west coast of India, and in a zone west of Sumatra due to freshening of the surface water caused by heavy precipitation. The haline buoyancy flux dominates in the central Arabian Sea due to evaporative cooling, where surface waters are pumped into the thermocline by Ekman convergence. During fall, the buoyancy flux is dominated by thermal component in the western Indian Ocean, but salt flux is a significant contributor to the surface buoyancy flux east of 80°E.

Summary and conclusion

Annual and seasonal variations in surface buoyancy flux in the tropical Indian Ocean were examined in the context of heat and freshwater fluxes across the air–sea interface.

Positive buoyancy flux regions are noted in the central Arabian Sea, south of 5°S, during summer, north-western Arabian Sea during winter, and a marked negative buoyancy flux north of 15°S, during spring. The buoyancy flux due to salt exceeds that due to heat in the north-western Arabian Sea during winter and in the Bay of Bengal during summer. The salt flux also shows dominance in the eastern equatorial Indian Ocean during summer and fall. This is due to excess evaporation and concomitant winter cooling in the northern Arabian Sea and due to excess precipitation in the Bay of Bengal and eastern equatorial Indian Ocean. The freshening at the surface would lead to an increase in total steric level and hence the geostrophic flow, if the freshwater is not carried away laterally. Thus, the present study reveals that the salt flux is a significant contributor to the surface buoyancy flux in the north Indian Ocean; this is due to evaporation in the Arabian Sea and due to precipitation in the Bay of Bengal, even though they occupy the same latitude belt, unlike in most other regions of the world oceans.

The hydrostatically unstable vertical distribution of salinity and temperature associated with evaporative

cooling (or winter cooling) in the northern Arabian Sea is expected to be the regions of convective formation of Arabian Sea High Salinity water mass^{3,15}. The formation of water mass must involve downward transport of heat and salt from the high salinity surface layer leading to the formation of salt fingers. A recent study by Prasanna Kumar and Prasad¹⁵ elucidated the physical forcing that led to the formation of Arabian Sea High Salinity Water mass and Madhupradap *et al.*¹⁶ have shown the mechanism of the biological response to winter cooling in the northern Arabian Sea.

1. Rochford, D. J., *Aust. J. Mar. Fresh. Res.*, 1964, **15**, 1–24.
2. Varkey, M. J., Ph D thesis, University of Kerala, 1986.
3. Prasanna Kumar, S. and Prasad, T. G., *Deep-Sea Res.*, 1997, in press.
4. Baumgartner, A. and Reichel, E., *The World Water Balance, Mean Annual Global, Continental and Maritime Precipitation Evaporation and Runoff*, Elsevier, 1975, p. 179.
5. Woodruff, S. O., Slutz, R. J., Jenne, R. L. and Steuver, P. M., *Bull. Am. Meteorol. Soc.*, 1987, **68**, 1239–1250.
6. Bunker, A. F., *Mon. Weath. Rev.*, 1976, **104**, 1122–1140.
7. Rao, A. V. R. K., Kelkar, R. R. and Arkin, P. A., *Mausam*, 1989, **40**, 123–130.
8. Ramesh Kumar, M. R. and Prasad, T. G., *J. Geophys. Res.*, 1997, in press.

9. Fofonoff, N. P. and Millard, R. C., *UNESCO Tech. Pap. Mar. Sci.*, 1984, **44**, 53.
10. Stern, M. W., *Ocean Circulation Physics*, Academic Press, 1975, p. 209.
11. Levitus, S. R., Gelfeld, R., Boyer, T. and Johnson, D., *Results of the NODC and IOC Oceanographic Data Archaeology and Rescue Projects. Key to Oceanographic Records Documentation*, NODC, Washington DC, 1994, No. 19.
12. Jaeger, L., *Ber. Dtsch. Wetterdienstes*, 1976, no. 139, 18.
13. Martin, D. W., Hinton, B. B. and Auvine, B. A., *Bull. Am. Meteorol. Soc.*, 1993, **74**, 581–590.
14. Rao, M. S. V., Abbott, W. V. and Theon, J. S., *Satellite-derived Global Oceanic Rainfall Atlas (1973 and 1974)*, NASA SP-410, Washington DC, 31, plus appendices, 1976.
15. Prasanna Kumar, S. and Prasad, T. G., *Curr. Sci.*, 1996, **71**, 834–841.
16. Madhupradap, M., Prasanna Kumar, S., Bhattathiri, P. M. A., Dileep Kumar, M., Raghukumar, S., Nair, K. K. and Ramaiah, N., *Nature*, 1996, **384**, 549–552.

ACKNOWLEDGEMENTS. I thank the India Meteorological Department for providing the INSAT precipitation data. I acknowledge financial support from DST, New Delhi, as part of TOGA-I program. I am also thankful to the anonymous referee for valuable suggestions.

Received 18 February 1997; revised accepted 12 September 1997.

Particle bombardment: A simple and efficient method of alfalfa (*Medicago sativa* L.) pollen transformation

Shashi M. Ramaiah¹ and Daniel Z. Skinner^{1,2}

Department of Agronomy¹ and USDA-ARS², Throckmorton Hall, Kansas State University, Manhattan, KS 66502-5501, USA

Direct delivery of DNA into pollen was used to obtain transgenic alfalfa (*Medicago sativa* L.). Plasmid pBI121 bearing the β -glucuronidase (GUS) reporter gene was introduced into the pollen by microprojectile bombardment. The bombarded pollen expressed GUS activity. Pollinating flowers of male-sterile plants with the bombarded pollen produced fertile seeds. Thirty per cent of plants derived from the fertile seeds showed integration of GUS plasmid, which was confirmed by PCR and Southern analysis. However, after ten vegetative generations, some

transgenic plants (T_0) apparently lost the integrated GUS plasmid, while in few others, GUS gene copy number decreased. Presently, we are not able to establish the possible causes for the loss of integrated DNA after several vegetative generations. However, it would be a worthwhile avenue for future work to establish the reasons for the loss of integrated DNA since this method of transformation employs simple techniques to transform pollen and produce transgenic plants through the natural plant reproductive process.

ALFALFA (*Medicago sativa* L.) is a highly valued forage legume crop cultivated worldwide on 32 million hectares in warm and cool subtropical regions^{1,2}. Improvements of alfalfa, earlier was restricted largely to conventional breeding methods. Recently, attempts to

genetically engineer alfalfa by plant transformation have relied on gene introduction techniques demanding tissue culture methods^{3–6}. Plant transformation methods involving tissue culture are time-consuming, require special techniques, and the efficiency of obtaining stable